Available online at www.sciencedirect.com
ScienceDirect
Geochimica et Cosmochimica Acta 74 (2010) 4639–4654
Geochimica et Cosmochimica Acta
www.elsevier.com/locate/gca

New indices and calibrations derived from the distribution of crenarchaeal isoprenoid tetraether lipids: Implications for past sea surface temperature reconstructions

Jung-Hyun Kim [a,*], Jaap van der Meer [a], Stefan Schouten [a], Peer Helmke [b], Veronica Willmott [a], Francesca Sangiorgi [c], Nalân Koç [d], Ellen C. Hopmans [a], Jaap S. Sinninghe Damsté [a]

[a] *NIOZ Royal Netherlands Institute for Sea Research, Department of Marine Organic Biogeochemistry (BGC) and Department of Marine Ecology (MEE), P.O. Box 59, 1790 AB, Den Burg, Texel, The Netherlands*
[b] *Federal Institute of Hydrology, Department of Water Balance, Forecasting and Predictions, Am Mainzer Tor 1, 560 Koblenz, Germany*
[c] *Biomarine Sciences, Institute of Environmental Biology, Faculty of Science, Utrecht University, The Netherlands*
[d] *Norwegian Polar Institute, Polar Environmental Centre, N-9296 Tromsø, Norway*

Received 23 November 2009; accepted in revised form 11 May 2010; available online 2 June 2010

Abstract

Several studies have shown that there is a strong relationship between the distribution of crenarchaeotal isoprenoid glycerol dibiphytanyl glycerol tetraethers (GDGTs) and sea surface temperature (SST). Based on this, a ratio of certain GDGTs, called TEX_{86} (TetraEther indeX of tetraethers consisting of 86 carbon atoms), was developed as a SST proxy. In this study, we determined the distribution of crenarchaeotal isoprenoid GDGTs in 116 core-top sediments mostly from (sub)polar oceans and combined these data with previously published core-top data. Using this extended global core-top dataset ($n = 426$), we re-assessed the relationship of crenarchaeal isoprenoid GDGTs with SST. We excluded data from the Red Sea from the global core-top dataset to define new indices and calibration models, as the Red Sea with its elevated salinity appeared to behave differently compared to other parts of the oceans. We tested our new indices and calibration models on three different paleo datasets, representing different temperature ranges. Our results indicate that the crenarchaeol regio-isomer plays a more important role for temperature adaptation in (sub)tropical oceans than in (sub)polar oceans, suggesting that there may be differences in membrane adaptation of the resident crenarchaeotal communities at different temperatures. We, therefore, suggest to apply two different calibration models. For the whole calibration temperature range (−3 to 30 °C), a modified version of TEX_{86} with a logarithmic function which does not include the crenarchaeol regio-isomer, called TEX_{86}^{L}, is shown to correlate best with SST: $SST = 67.5 \times TEX_{86}^{L} + 46.9$ ($r^2 = 0.86$, n=396, p <0.0001). Application of TEX_{86}^{L} on sediments from the subpolar Southern Ocean results in realistic absolute SST estimates and a similar SST trend compared to a diatom SST record from the same core. TEX_{86}^{H}, which is defined as the logarithmic function of TEX_{86}, yields the best correlation with SST, when the data from the (sub)polar oceans are removed: $SST = 68.4 \times TEX_{86}^{L} + 38.6$ ($r^2 = 00.87$, $n = 255$, $p < 0.0001$). Furthermore, TEX_{86}^{L} gives the best correlation for mescosm data with temperatures ranging between 10 and 46 °C. For Quaternary sediments from the tropical Arabian Sea, both TEX_{86}^{L} and TEX_{86}^{H} yield similar trends and SST estimates. However, the extrapolation of TEX_{86}^{H} calibration on a sediment record from a greenhouse world ocean predicts more reliable absolute SST estimates and relative SST changes in agreement with estimates based on the $\delta^{18}O$ of planktonic foraminifera. Based on the comparison of TEX_{86}^{L} and TEX_{86}^{H} derived SSTs using the core top data, we recommend applying TEX_{86}^{H} above 15 °C

* Corresponding author. Tel.: +31 (0) 222 369567; fax: +31 (0) 222 319674.
E-mail address: Jung-Hyun.Kim@nioz.nl (J.-H. Kim).

doi:10.1016/j.gca.2010.05.027

and TEX_{86}^{L} below 15 °C. In cases where paleorecords encompass temperatures both below and above 15 °C, we suggest to use TEX_{86}^{L}.

1. INTRODUCTION

In the marine water column, isoprenoid glycerol dibiphytanyl glycerol tetraethers (GDGTs) are mainly biosynthesized by Marine Group I Crenarchaeota, which are one of the dominant prokaryotes in today's oceans (e.g. Karner et al., 2001; Herndl et al., 2005). Marine Group I Crenarchaeota biosynthesize different types of isoprenoid GDGTs containing 0–3 cyclopentane moieties (Fig. 1) and crenarchaeol which, in addition to 4 cyclopentane moieties, contains a cyclohexane moiety (Schouten et al., 2000, 2008; Sinninghe Damsté et al., 2002). In addition, they also biosynthesize a regio-isomer of crenarchaeol. Schouten et al. (2002) introduced TEX_{86} (TetraEther indeX of tetraethers consisting of 86 carbon atoms) as a sea surface temperature (SST) proxy based on the relative abundance of isoprenoid GDGTs:

$$TEX_{86} = \frac{[GDGT-2] + [GDGT-3] + [Cren']}{[GDGT-1] + [GDGT-2] + [GDGT-3] + [Cren']} \quad (1)$$

where GDGT-1, GDGT-2, and GDGT-3 indicate GDGTs containing 1, 2, and 3 cyclopentane moieties, respectively, and Cren' the crenarchaeol regio-isomer (Fig. 1). The definition of this ratio is based on the fact that the number of cyclopentane moieties increase with increasing temperature and this index was shown to correlate best with annual mean SST in a relatively small set ($n = 44$) of core-top data. Schouten et al. (2002) excluded the two most abundant isoprenoid GDGTs (GDGT-0 and crenarchaeol) from the TEX_{86} definition to avoid their overpowering influence on the index as their abundance was generally much higher than that of the other GDGTs. GDGT-0 was also excluded as it was known to be also sourced by other Archaea, such as methanogenic and methanotrophic Euryarchaeota, especially those living in anoxic sedimentary environments (e.g. Pancost et al., 2001). However, Schouten et al. (2002) did not perform a rigorous statistical evaluation to show that TEX_{86} is the index correlating best with SST.

Recently, the initial linear core-top calibration of TEX_{86} of Schouten et al. (2002) has been updated using a more extensive, global core-top dataset ($n = 284$, Kim et al.,

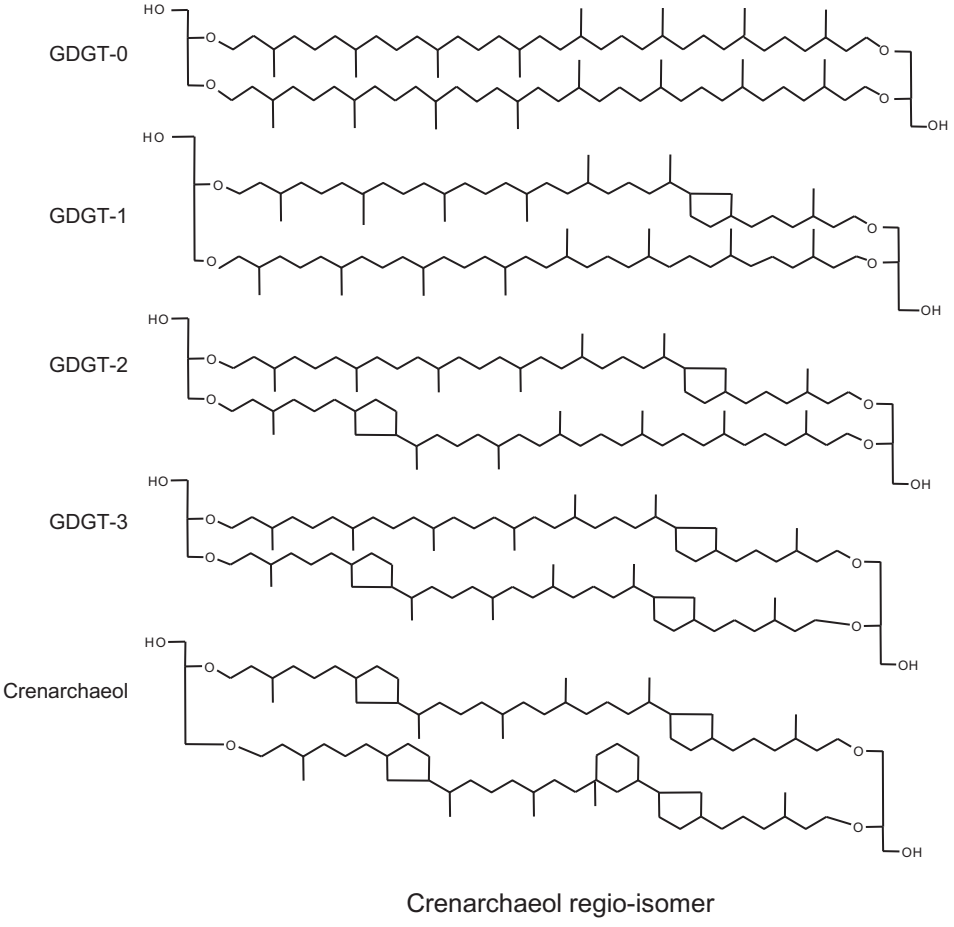

Fig. 1. Structures of isoprenoid GDGTs discussed in the text.

Table 1
Isoprenoid GDGT indices and calibration models based on newly extended global core-top data and mesocosm data from Wuchter et al. (2004) and Schouten et al. (2007a).

	Temp. range (°C)	Eq. (#)	Equation	Data points (n)	Determination coefficient (r^2)	Residual standard error (°C, ±1σ)	References
Global core-top calibration model (0 m)	5 to 30	2	$T = 56.2 \times TEX_{86} - 10.8$	223	0.94	1.7	Kim et al. (2008)
New calibration models							
Core-top:							
TEX_{86} linear calibration model (0 m)	−3 to 30	5	$T = 81.5 \times TEX_{86}$ - 26.6	396	0.77	5.2	This study
TEX_{86} reciprocal calibration model (0 m)	−3 to 30	6	$T = -19.1 \times (1/TEX_{86}) + 54.5$	396	0.75	5.4	This study
GDGT index-1 calibration model (0 m)	−3 to 30	8	$T = 67.5 \times$ (GDGT index-1) + 46.9	396	0.86	4.0	This study
GDGT index-2 calibration model (0 m)	5 to 30	10	$T = 68.4 \times$ (GDGT index-2) + 38.6	255	0.87	2.5	This study
Mesocosm:							
TEX_{86} linear calibration model	10 to 40	11	$T = 48.2 \times TEX_{86} + 1.04$	21	0.85	3.3	This study
TEX_{86} reciprocal calibration model	10 to 40	12	$T = -9.0 \times (1/TEX_{86}) + 45.2$	21	0.77	4.1	This study
GDGT index-1 calibration model	10 to 40	13	$T = 42.9 \times$ (GDGT index-1) + 46.5	21	0.62	5.5	This study
GDGT index-2 calibration model	10 to 40	14	$T = 52.0 \times$ (GDGT index-2) + 42.0	21	0.84	3.4	This study

2008). This new calibration study supports the initial finding that TEX_{86} reflects mostly annual mean temperatures of the upper mixed layer of the ocean. It showed that for SSTs between 5 and 30 °C TEX_{86} is linearly correlated with SST as follows (Eq. (2), Table 1):

$$SST = 56.2 \times TEX_{86} - 10.8 \quad (r^2 = 0.935, n = 223) \qquad (2)$$

However, this study also revealed that the relationship between TEX_{86} values and SSTs over the entire temperature range (−2 to 30 °C) is non-linear, mainly because below 5 °C, i.e. in the polar oceans, changes in TEX_{86} are relatively minor with temperature. Therefore, Kim et al. (2008) suggested that the TEX_{86} proxy might not be directly applicable for the polar oceans. Recently, Liu et al. (2009) used the data of Kim et al. (2008) to suggest an alternative non-linear calibration for TEX_{86}:

$$SST = -16.332 \times (1/TEX_{86}) + 50.475 \quad (r^2 = 0.817, n = 287) \qquad (3)$$

In this study, we analysed the GDGT distribution of a substantial number (116) of new core-tops from (sub)polar oceans for a better spatial coverage of the core-top dataset by Kim et al. (2008). Furthermore, we used satellite-derived SST rather than SST data from the World Ocean Database (WOD) because the resolution of the WOD dataset is often too low to determine the temperature signal of local sites close to the coasts. We also performed statistical analyses to examine the relation of the different isoprenoid GDGTs with SST. The results were then used to establish new indices and calibration models. Finally, we assessed the applicability of these new indices and calibration models for paleoclimate studies by applying them to sediment cores from three different regions of which TEX_{86} SST records were previously published.

2. MATERIALS AND METHODS

2.1. Core-top sediments and satellite-derived SST data

Marine core-tops analyzed in this study were collected mostly using box- and multi-corers from various parts of the world oceans and different water depths. They represent the uppermost layer, mostly 0–1 cm. In this study, we analyzed 116 core-tops mostly from (sub)polar oceans. In addition, data from previously analyzed core-tops from the Red Sea (see Trommer et al., 2009 for details) were added to the new global core-top dataset. In total, the dataset comprises 426 core-tops from various oceans (Fig. 2, see also Electronic Annex). Although the global core-top data are dominated by continental margin sediments, they all contain relatively low amounts of soil-derived branched GDGTs, i.e. the Branched Isoprenoid Tetraether Index (Hopmans et al., 2004) shows values below 0.3 (cf. Weijers et al., 2006). Thus, the TEX_{86} values are unlikely to be biased by soil organic matter input.

SST data of each sampling site were retrieved from the NSIPP AVHRR Pathfinder and Erosion Global 9 km SST Climatology dataset for the period of 1985–1995 from the Physical Oceanography Distributed Active Archive Center at NASA Jet Propulsion Laboratory, Pasadena, CA (Casey and Cornillon, 1999). We used 10-yr average values of the annual mean climatology SST data to explore

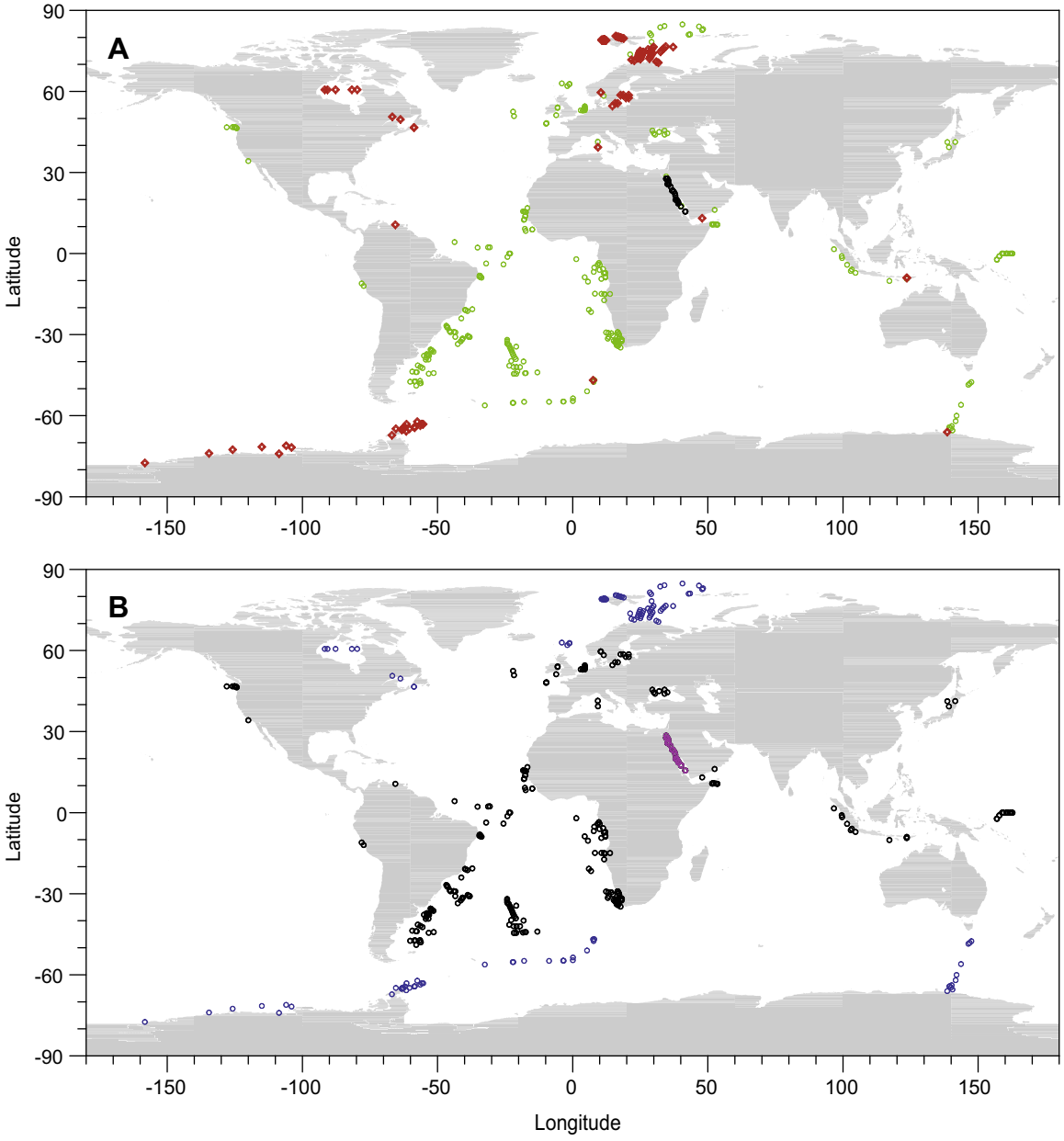

Fig. 2. Locations of the core-top sediments considered in this study. In panel A, green and black circles indicate the core-tops used in the previous studies by Kim et al. (2008) and Trommer et al. (2009), respectively and red diamonds newly added core-tops in this study. In panel B, open circles indicate core-tops from (sub)tropical areas, blue circles from (sub)polar oceans, and purple circles from the Red Sea (see Statistical analysis in Material and methods). (For interpretation of the references to color in this figure legend, the reader is referred to the web version of this paper.)

the relationships of the distribution of isoprenoid GDGTs with SST.

2.2. GDGT extraction and purification

Sediments (1–5 g) were freeze-dried and homogenized by mortar and pestle. The sediments were extracted by Dionex™ accelerated solvent extraction (DIONEX ASE 200) using a mixture of dichloromethane (DCM)/methanol (MeOH) (9:1, v/v) at a temperature of 100 °C and a pressure of 7.6×10^6 Pa. The extracts were separated by Al_2O_3 column chromatography using hexane/DCM (9:1, v/v), hexane/DCM (1:1, v/v) and DCM/MeOH (1:1, v/v) as subsequent eluents. The polar fraction (DCM/MeOH) was concentrated under N_2, dissolved in hexane/isopropanol (99:1, v/v), and filtered using a 0.4 μm PTFE filter prior to injection as described by Hopmans et al. (2000, 2004).

2.3. GDGT analysis

Analyses were performed using an Agilent (Palo-Alto, CA, USA) 1100 series LC-MS equipped with an auto-injec-

tor and Chemstation chromatography manager software (see Hopmans et al., 2000 and Schouten et al., 2007b). Separation was achieved on a Prevail Cyano column (2.1 × 150 mm, 3 μm; Alltech, Deerfield, IL, USA), maintained at 30 °C. Injection volumes varied from 1 to 20 μl. GDGTs were eluted isocratically with 99% A and 1% B for 5 min, followed by a linear gradient to 1.8% B in 45 min, where A = hexane and B = propanol. Flow rate was 0.2 ml/min. After each analysis the column was cleaned by back-flushing hexane/propanol (90:10, v/v) at 0.2 ml/min for 10 min. Detection was achieved using atmospheric pressure positive ion chemical ionization mass spectrometry (APCI-MS). Conditions for the HP 1100 APCI-MS were as follows: nebulizer pressure 60 psi, vaporizer temperature 400 °C, drying gas (N_2) flow 6 l/min and temperature 200 °C, capillary voltage −3 kV, corona 5 μA (~3.2 kV). GDGTs were detected by Selected Ion Monitoring (SIM) of their $[M+H]^+$ ions (dwell time = 234 ms) (Schouten et al., 2007b). Fractional abundances of each isoprenoid GDGT component were obtained by normalizing each peak area to the summed area of all six isoprenoid GDGTs.

2.4. Statistical analysis

Firstly, we performed a Principal Component Analysis (PCA) on the isoprenoid GDGT data to identify outliers. Secondly, indices based on the isoprenoid GDGT data were defined as a proxy for SST. In other words, a calibration equation that converts an index value into SST was established. Since both SST and GDGT data were obtained from a sample, the calibration is a so-called natural calibration case (Brown, 1993), implying that a simple linear regression analysis where SST is the dependent variable and the index the independent variable, will provide a calibration equation. We have chosen to select a simple index of the following form:

$$\text{GDGT index} = \log\frac{\sum_{k1} Y_j}{\sum_{k2} Y_j} \quad (4)$$

Y_j refers to one of the six isoprenoid GDGTs. For example, Y_1 refers to GDGT-0. The summation in the numerator and the denominator is over the sets *k1* and *k2*, respectively. A set can be any possible combination of isoprenoid GDGTs. For example, the combination of GDGT-0, GDGT-2, and crenarchaeol is a possible set. The aim was then to select those sets *k1* and *k2* for which the accompanying index reveals the largest squared correlation r^2 (or explained variance) with SST. We tested all possible combinations of *k1* and *k2*. With 6 isoprenoid GDGTs, there are 63 different sets (6 of a single isoprenoid GDGT, 15 of two isoprenoid GDGTs, 20 of three isoprenoid GDGTs, 15 of four isoprenoid GDGTs, 6 of five isoprenoid GDGTs, and 1 that contains all six isoprenoid GDGTs). Hence 63x62/2 or 1953 relevant combinations were tested.

A log-ratio is generally preferable over an ordinary ratio, since it usually makes the error structure closer to a normal distribution with constant variance (e.g. Montgomery and Peck, 1992). We checked for normality and homogeneity of variance by inspection of the residual plots. We used the R package (R Development Core Team, 2008) for all our statistical analyses.

3. RESULTS AND DISCUSSION

All six isoprenoid GDGT components were detected in the newly analyzed 116 core-top sediments in this study. These data substantially improved the spatial coverage for (sub)polar oceans compared to our previous study (Kim et al., 2008) (Fig. 2). These new core-top data were then combined with previously obtained core-top data (Kim et al., 2008; Trommer et al., 2009) and the new, extended, global dataset comprised 426 core-tops from various oceans. We performed statistical analyses on the fractional abundances of the six isoprenoid GDGTs and the results are discussed below.

3.1. Relation of individual isoprenoid GDGTs with SST

The PCA shows that the first two PCs explain 94.1% of the variation of the data. On the PC1 axis (explaining 76.5% of the variance), GDGT-0 is negatively correlated with all the other GDGTs (Fig. 3). On the PC2 axis (explaining 17.6% of the variance), GDGT-3, crenarchaeol, and its regio-isomer are negatively correlated with the other GDGTs. In this PCA, the Red Sea data clusters as a distinct group separated from the other data. This suggests that the Red Sea behaves differently compared to other ocean basins. Indeed, Trommer et al. (2009) showed that isoprenoid GDGT distributions, especially in the northern Red Sea, responded differently with respect to SST than found in other parts of the oceans. Crenarchaeota thriving in the Red Sea probably represent a different population with a different temperature response due to the extreme conditions in this enclosed basin, i.e. high evaporation and thus high salinity.

We then examined the relationships of the fractional abundances of individual GDGTs with SST (Fig. 4). This

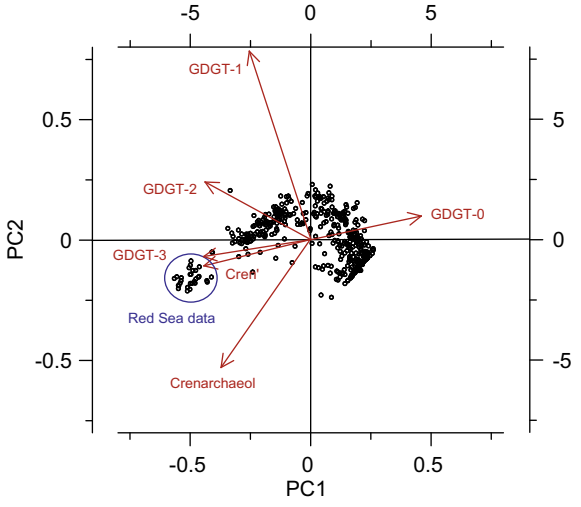

Fig. 3. Triplots of the PCA ($n = 426$). The first two PCs explain 92.6% of the variation of the data. Closed circles and red lines represent scores and response variables (isoprenoid GDGTs), respectively. (For interpretation of the references to colour in this figure legend, the reader is referred to the web version of this article.)

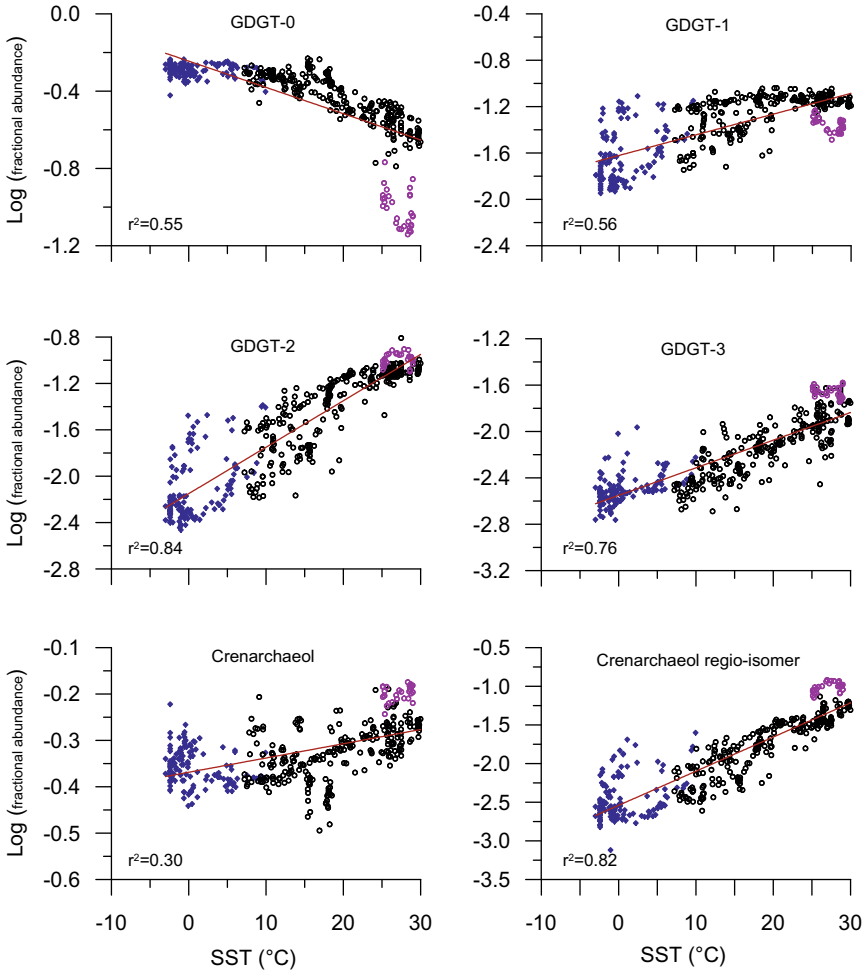

Fig. 4. Correlation of the fractional abundance of individual isoprenoid GDGTs obtained by normalizing each peak area to the summed area of all six isoprenoid GDGTs with satellite-derived SST. Symbols and colors are as in Fig. 2B.

comparison shows that only the fractional abundance of GDGT-0 has a negative correlation with SST ($r^2 = 0.55$), while other components have positive slopes with low to high determination coefficients ($r^2 = 0.3$–0.84). Crenarchaeol has the poorest correlation with SST ($r^2 = 0.3$). These results suggest that the fractional abundances of GDGTs with cyclopentane moieties increase with higher SSTs, while that of GDGT-0 decreases.

3.2. Core-top calibration models

We first explored the relationship of TEX_{86} values of the extended global core-top data with SST for the entire temperature range from −3 to 30 °C (Fig. 5A). We excluded the Red Sea data from the global core-top dataset for statistical analyses as the Red Sea behaves differently compared to other ocean basins as discussed above and is thus not representative of GDGT distributions in open ocean settings (see also Fig. 3). The resulting equation (Fig. 5A, Table 1) is as follows:

$$\mathrm{SST} = 81.5 \times \mathrm{TEX}_{86} - 26.6 \ (r^2 = 0.77, n = 396, p < 0.0001) \quad (5)$$

A strong correlation (determination coefficient $r^2 = 0.77$) is observed, confirming that this proxy contains a strong temperature signal. ANOVA tests confirm the linear relationship for this calibration model ($p < 0.0001$). However, a large scatter can be observed at low temperatures (<5 °C). This confirms the previous study by Kim et al. (2008), which showed a non-linear behavior of TEX_{86} at temperatures below 5 °C.

Recently, Liu et al. (2009) proposed a non-linear (reciprocal) calibration for TEX_{86}, using the global core-top dataset of Kim et al. (2008). We applied the same approach to our new global dataset and obtained the following equation (Fig. 5B):

$$\mathrm{SST} = -19.1 \times (1/\mathrm{TEX}_{86}) + 54.5 \ (r^2 = 0.75, n = 96, p < 0.0001) \quad (6)$$

This approach reveals a slightly worse correlation ($r^2 = 0.75$) than that of the linear calibration.

We further explored alternative indices to better describe a relationship between SST and GDGTs, especially to overcome the non-linearity and large scatter in the low and high temperature ranges. GDGT-0 can be biosynthesized not only by planktonic non-thermophilic Crenarchaeota (e.g.

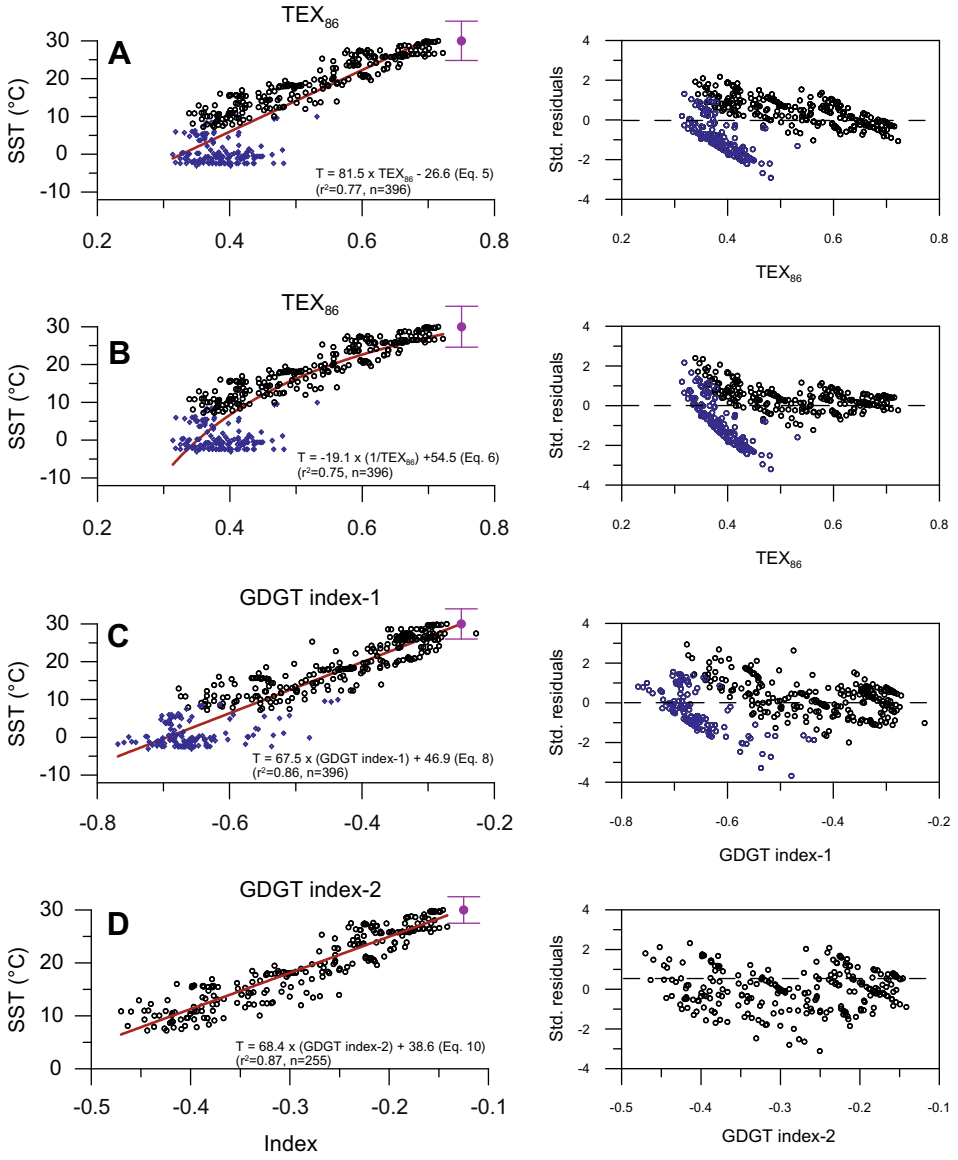

Fig. 5. Correlation of GDGT indices obtained from the core-top data with satellite-derived SST: (A) TEX_{86} as a linear function, (B) TEX_{86} as a reciprocal function and (C) GDGT index-1, and (D) GDGT index-2. Purple bards in left panels indicate residual standard error ($\pm 1\sigma$). Std. residuals denote standardized residuals. Symbols and colors are as in Fig. 2B.

Sinninghe Damsté et al. 2002; Schouten et al., 2008) but also specifically by methanogenic (e.g. Koga et al., 1993) and methanotrophic Archaea (e.g. Pancost et al., 2001), which are present in anoxic environments. In addition, GDGT-0 is generally one of the most abundant isoprenoid GDGTs in soils (Weijers et al., 2007) and thus GDGT-0 contributed by soil organic matter input could have more substantial influence on GDGT indices that include GDGT-0. These were the major reasons why GDGT-0 was not included in the TEX_{86} definition (cf. Schouten et al., 2002). Based on the same grounds, we decided to exclude GDGT-0 from further statistical analyses. Accordingly, we computed all possible combinations based on the remaining five GDGTs from the residual core top data ($n = 396$). The index that correlates best with SST (Fig. 5C) is as follows:

$$\text{GDGT index} - 1 = \log\left(\frac{[\text{GDGT} - 2]}{[\text{GDGT} - 1] + [\text{GDGT} - 2] + [\text{GDGT} - 3]}\right) \quad (7)$$

$$\text{SST} = 67.5 \times (\text{GDGT index}) + 46.9 \ (r^2 = 0.86, n = 396, p < 0.0001) \quad (8)$$

Interestingly, in contrast to TEX_{86}, GDGT index-1 does not contain the crenarchaeol regio-isomer. Furthermore, the determination coefficient is significantly higher than those of both linear and non-linear TEX_{86} calibration models.

To convert values of GDGT indices to SSTs beyond the present-day open-ocean systems (i.e., >30 °C), we need to extrapolate the global calibration lines. However, a

previous study (Schouten et al., 2003) showed that at SSTs above 30 °C, the reconstructed TEX_{86} values were higher than predicted by the global linear correlation line (Schouten et al., 2002). Accordingly, a calibration line using only a subset of the available data (>20 °C) provided more realistic SST estimates for the Cretaceous greenhouse world. Based on this approach, we performed the same statistical analyses but in addition to the Red Sea data, we also excluded data from (sub)polar oceans, where TEX_{86} is not changing with temperature (Kim et al., 2008). Again, the best combination was calculated based on five GDGTs, i.e. excluding GDGT-0. The resulting combination and correlation (Fig. 5D) with highest determination coefficients are as follows:

$$\text{GDGT index} - 2 = \log\frac{[\text{GDGT} - 2] + [\text{GDGT} - 3] + [\text{Cren'}]}{[\text{GDGT} - 1] + [\text{GDGT} - 2] + [\text{GDGT} - 3] + [\text{Cren'}]} \quad (9)$$

$$\text{SST} = 68.4 \times (\text{GDGT index} - 2) + 38.6 \ (r^2 = 0.87, \ n = 255, p < 0.0001) \quad (10)$$

Remarkably, the resulting best combination of isoprenoid GDGTs now includes the crenarchaeol regio-isomer and is in fact exactly the same as TEX_{86} but with a logarithmic function, i.e. $\log TEX_{86}$.

Our results suggest the need for two different calibration models for different temperature ranges, mainly because the relative abundance of the regio-isomer of crenarchaeol is strongly correlated with SST at high but not at low SST (Fig. 4). Therefore, the best fit combination of GDGTs with SST including all data does not contain this GDGT, whereas GDGT index-2 includes the crenarchaeol regio-isomer. It thus seems that, GDGT index-1, which does not include the crenarchaeol regio-isomer, is more appropriate for (sub)polar oceans, whereas GDGT index-2 seems better suitable for the determination of SST in (sub)tropical oceans. The apparently different role of crenarchaeol regio-isomer in the different provinces of the oceans may be due to the different relative abundance of this component in genetically distinct Crenarchaeota (see below). Furthermore, the concentration of the regio-isomer of crenarchaeol is often so small in (sub)polar oceans that the error in the quantification of its fractional abundance becomes large.

3.3. Accuracy of SST estimates

An important aspect of paleothermometers is the relative accuracy with which temperatures may be estimated. The main sources of error are the analytical error and those arising from the scatter in calibration of the indices with SST. For the global core-top dataset, using duplicate or triplicate analyses of 188 core-top samples, the median values of the standard deviation were estimated to be 0.004, 0.004, 0.003 for TEX_{86}, GDGT index-1, and GDGT index-2, respectively, corresponding to 0.3, 0.2, and 0.2 °C (Fig. 6). This might explain some of the scatter in standardized residuals (Fig. 5). Typically, values higher than $\pm 2\sigma$ standardized residuals indicate a poor fit of the regression

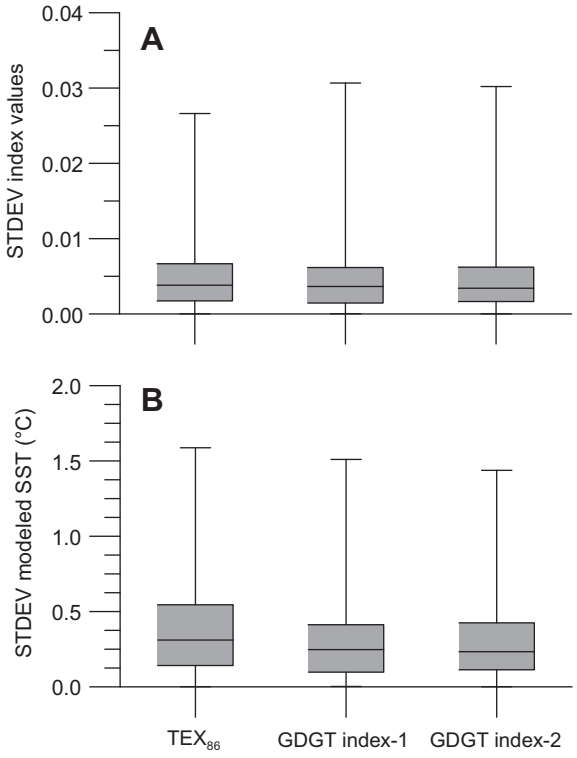

Fig. 6. Box-whisker plots showing minimum, maximum, median, lower quartile (25%), and upper quartile (75%) information for the standard deviation (STDEV) data ($n = 184$) of A) GDGT-based indices and B) modeled SSTs derived from the calibration models of (Eqs. (5), (8), and (10)) for TEX_{86}, GDGT index-1, and -2, respectively.

model. We calculated residual standard error (standard error of the estimate), which is a measure of the amount of error in the prediction of y (SST) for an individual x (index value). The standard error in temperature estimate using the GDGT index-1 calibration model (Eq. (8)) is 4.0 °C and using the GDGT index-2 calibration model (Eq. (10)) 2.5 °C (Table 1). The much lower error in GDGT index-2 compared to GDGT-index-1 is mostly due to the removal of the large scatter in the (sub)polar ocean dataset. However, it should be noted that if GDGT index-1 and -2 are calibrated on the same (sub)tropical dataset, the correlation of GDGT index-2 with SST is better than that of GDGT index-1 ($\text{SST} = 53.5 \times \text{GDGT index-1} + 42.1$, $r^2 = 0.80$, $n = 255$, $p < 0.0001$). The corresponding estimation error of GDGT index-2 is lower than that of GDGT index-1 (3.0 °C).

The standard errors for GDGT index-1 and -2 are higher than that of the TEX_{86} calibration model (Eq. (2)) as reported by Kim et al. (2008). However, it should be noted that for the calibration model by Kim et al. (2008), the calibration dataset was adjusted by removing outliers defined as $>\pm 1\sigma$ standardized residuals in addition to all data from the (sub)polar oceans and the Red Sea. For the new calibration models in this study, we did not adjust our dataset similar to Kim et al. (2008), resulting in no additional data removal from final calibration dataset. For example, our

calibration dataset for GDGT index-1 excludes 7% of the core-top data, while Kim et al. (2008) approach results in removal of 12% of the available calibration data. This may be at least partly a reason why the estimation error in temperature from the new linear calibration models (Eqs (8) and (10)) are higher.

It should be noted that residual standard errors comprise several other sources in addition to analytical errors. Firstly, seasonal differences of crenarchaeotal production in the different oceanic settings may account for some of the scatter and thus increase SST prediction errors. To explore to what extent the global core-top signals are influenced by seasonality of crenarchaeotal production, we correlated GDGT index-1 values against both summer and winter mean SSTs (data not shown). The core-top GDGT index-1 values are highly correlated to both seasonal mean temperatures although the r^2 value for winter (0.88, $p < 0.0001$) is slightly higher than that for summer (0.80, $p < 0.0001$). This suggests that crenarchaeotal production of GDGTs more often takes place in winter. Indeed, Herfort et al. (2006) showed that the TEX_{86} values in North Sea sediments primarily reflected winter temperatures, in agreement with higher GDGT concentrations in core lipids (Wuchter et al., 2005) and higher abundance of Crenarchaeota (Wuchter et al., 2006a) in surface waters in that season. Furthermore, Wuchter et al. (2006b) showed that the TEX_{86} signal of particulate organic matter in sediment traps at 500 m varied with seasonal SST in the Arabian Sea. This is probably causing most of the scatter seen in the calibration plots (Fig. 5). However, it is not possible at this stage to estimate the offset relative to annual mean SST for each core-top location because we lack data on the seasonal abundance of Marine Group I Crenarchaeota in the different oceanic provinces and data on water column GDGT fluxes. Secondly, the varying depth of Marine Group I Crenarchaeota production might be another reason for the observed scatter. For instance, Huguet et al. (2007a, b) observed that TEX_{86} values in sediment traps and a sediment core in the Santa Barbara basin reflected subsurface temperatures (100–150 m) rather than SST. Kim et al. (2008) and Lee et al. (2008) also observed that TEX_{86} in upwelling areas might underestimate SSTs possibly as crenarchaeotal production might be greater in deeper water depth than in surface. Again, it is impossible to assess the production depth of isoprenoid GDGTs for all the individual core-top locations. Thirdly, lateral transport of GDGTs attached to fine-grained particles from remote areas with potentially different SST may contribute to increased standard errors of temperature estimate. Recently, we (Kim et al., 2009) investigated the effect of such lateral transport on the $U_{37}^{K'}$ and TEX_{86} proxies in the Southern Ocean and showed that there was a good similarity between the TEX_{86} SST record and the foraminifera and diatom SST records on the one hand but a strong dissimilarity with the $U_{37}^{K'}$ SST record. This finding was in good agreement with the hypothesis that isoprenoid GDGTs are less refractory than alkenones and that, therefore, isoprenoid GDGT distributions are less affected by lateral transport than those of alkenones (Mollenhauer et al., 2007, 2008; Shah et al., 2008). This suggests that GDGT-based proxies are primarily influenced by local conditions and less subject to long-distance lateral transport and, thus, this factor probably does not play a dominant role in the observed scatter. Finally, additional contribution of isoprenoid GDGTs produced by other archaeal communities than Marine Group I Crenarchaeota in the water column or sediment (e.g. Lipp et al., 2008; Lipp and Hinrichs, 2009) or from soil erosion (Weijers et al., 2006) may distort temperature signals in GDGT-based indices. For example, isoprenoid GDGT 1-3 are found in methane-oxidizing Euryarchaeota living in anoxic environments (e.g. Pancost et al. 2001; Blumenberg et al. 2004) and isoprenoid GDGTs, albeit in low relative amounts, are found in soil (Weijers et al., 2006). However, the latter does not likely bias GDGT indices, if BIT values are well below 0.3 (Weijers et al., 2006).

3.4. Testing the new indices on mesocosm and culture data

Using mesocosms, Wuchter et al. (2004) and Schouten et al. (2007a) showed that the crenarchaeotal membrane composition responded to growth temperatures between 10 and 40 °C in enrichment cultures and that there was a linear correlation of TEX_{86} with growth temperature. We tested our new indices (GDGT index-1 and -2, see above) together with TEX_{86} both as a linear function (cf. Kim et al., 2008) and as a reciprocal function (cf. Liu et al., 2009). In addition, we plotted three data points obtained from GDGT analysis of the biomass of *Candidatus Nitrososphaera gargensis* cultivated at 42, 46 and 52 °C (Pitcher et al., 2010) and one data point from *Candidatus* "*Nitrosopumilus maritimus*" cultivated at 28 °C (Schouten et al., 2008). Note that the latter data points are not included in the calibration models presented in Fig. 7 (see below).

All four indices derived from the GDGT composition in the mesocosm data show in general a strong positive relationship with incubation temperatures ($r^2 = 0.60$ to 0.85). GDGT index-1 shows the weakest correlation ($r^2 = 0.60$). Interestingly, the three data points of Ca. *N. gargensis* (Pitcher et al., 2010) do not fall closely to the mesocosm calibration lines of GDGT index-1 but instead agree well with that of TEX_{86} when plotted as a linear function of temperature and with GDGT index-2 (log TEX_{86}). However, these culture data do not plot closely on the reciprocal calibration line (cf. Liu et al., 2009) of TEX_{86}, suggesting that this type of calibration is not suitable for estimating high temperatures. The single data point of Ca. "*N. maritimus*" cultured at 28 °C (Schouten et al., 2008) fits well to all calibration lines.

The correlation of GDGT index-2 (log TEX_{86}) values obtained from these mesocosm experiments with incubation temperatures has a different slope and intercept compared to the core-top based equation (see Figs. 5 and 7). This is probably, at least in part, due to lower relative abundance of the regio-isomer of crenarchaeol in the mesocosm series (typically <1%) than in the core-tops from the subtropical to tropical regions (generally >1%), as noted previously by Wuchter et al. (2004) and Schouten et al. (2007a). At present, it is not clear why Marine Group I Crenarchaeota enriched in those mesocosm experiments produced less crenarchaeol regio-isomer than in natural

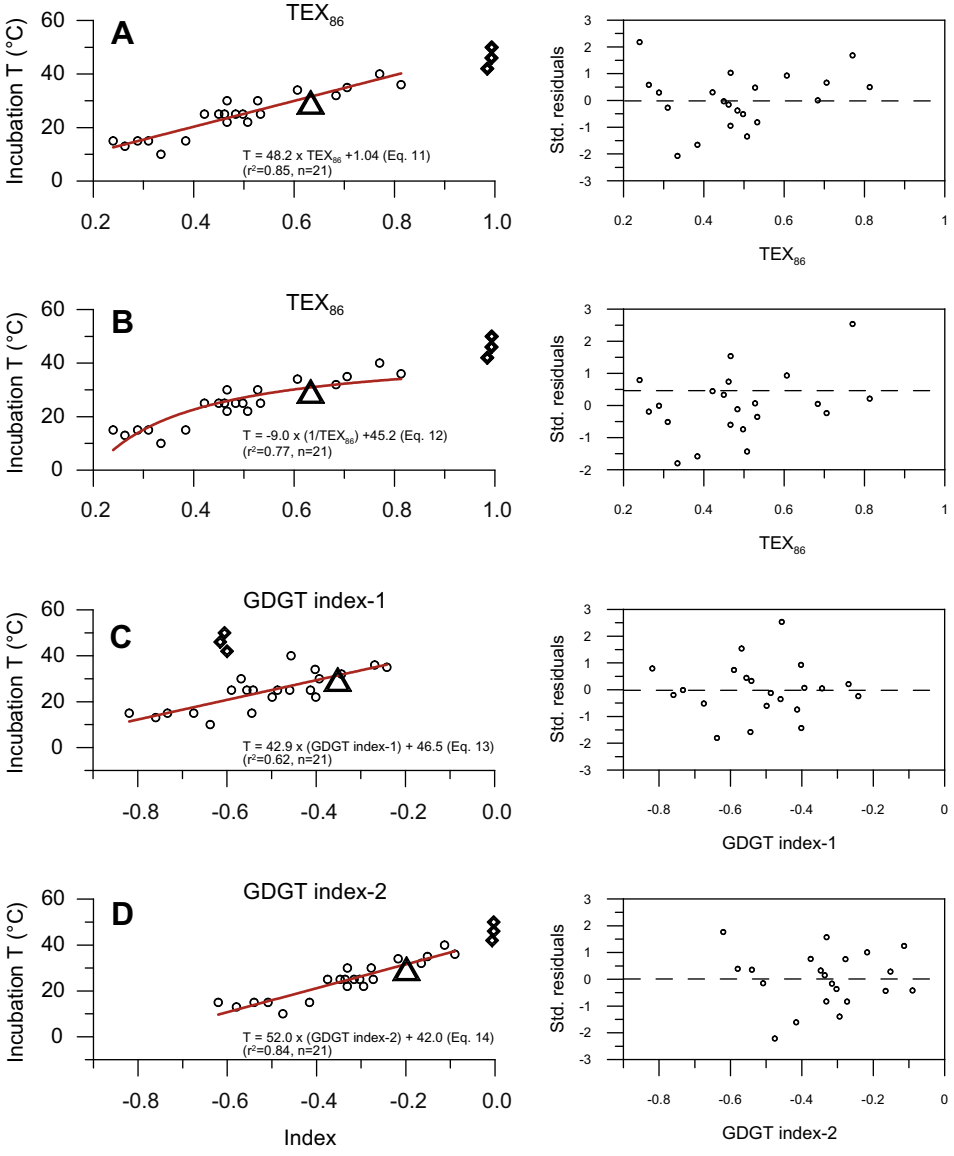

Fig. 7. Correlation of GDGT indices acquired from the mesocosm and culture data (Wuchter et al., 2004; Schouten et al., 2007a, 2008; Pitcher et al., 2010) with incubation temperatures: (A) TEX_{86} as a linear function, (B) TEX_{86} as a reciprocal function and (C) GDGT index-1, and (D) GDGT index-2. Std. residuals denote standardized residuals. Diamonds and triangle indicate data points of Ca. *N. gargensis* (Pitcher et al., 2010) and of Ca. *N. maritimus* (Schouten et al., 2008).

environments but we may speculate that Marine Group I Crenarchaeota species in the enrichment cultures are not completely representative of those occurring in nature. In contrast, Ca. N. gargensis, isolated from a hot spring microbial mat (Hatzenpichler et al., 2008), produced a much larger amount of crenarchaeol regio-isomer up to 24% (Pitcher et al., 2010). Shifts in the crenarchaeotal community structure in the mesocosm experiments were observed with temperature but no dramatic shifts in TEX_{86} values were observed (Schouten et al., 2007a). Similarly, different Crenarchaeota species may flourish in diverse temperature and oceanographic settings, possibly producing different amount of crenarchaeol regio-isomer and responding differently to SST than in the mesocosm experiments. This perhaps would also explain the different correlations of GDGT distributions with SST in the (sub)polar oceans, (sub)tropical regions, and the Red Sea. Recently, Shah et al. (2008) showed that in marine sediments from the Santa Monica basin the crenarchaeol regio-isomer was more depleted in $\Delta^{14}C$ relative to other isoprenoid GDGTs. This might be another hint that the concentration of crenarchaeol regio-isomer is not only governed by temperature. However, further study is needed to verify this result.

3.5. Testing the new indices using paleo data

To test the impact of our new indices and calibration models on past SST reconstructions, we applied them to three different datasets, representing different temperature ranges.

3.5.1. (Sub)polar oceans

Quaternary sediments (core MD88-769) recovered from the Southern Ocean (46°04′S, 90°06′E, water depth 3400 m; Kim et al., 2009) were used to reconstruct SST changes in the subpolar ocean. The present-day annual mean SST at the core site is 9 °C, while summer and winter mean SSTs are 9.4 and 7.7 °C, respectively (Casey and Cornillon, 1999). Summer SST estimated from diatom assemblages for MD88-769 ranged from 6 to 9 °C between 50 and 23 ka and from 5 to 7 °C during the Last Glacial Maximum (Fig. 8A; Kim et al., 2009). The TEX_{86} SSTs calculated using the new TEX_{86} calibration (Eq. (5)) were on average 3 °C during the last glacial period. This estimate is much lower than 10 °C derived from the previous TEX_{86} calibration model (Kim et al., 2008). However, as discussed before, the TEX_{86} calibration model (both the linear function, Eq. (5), as well as the reciprocal function, Eq. (6) does not resolve a large scatter below 5 °C. The GDGT index-2 calibration model, which includes the crenarchaeol regioisomer and is based on data from non-(sub)polar oceans only, yields warmer SST estimates in comparison to other calibration models, showing that it is, as expected, not applicable in this temperature regime. In contrast, application of GDGT index-1 (Fig. 8A) reveals a trend and absolute SST estimates that fit well with the diatom-derived SSTs (Kim et al., 2009). In (sub)polar oceans, diatoms grow in spring/summer with hardly any production during the winter period. The buried diatoms in sediments are, therefore, for the largest part derived from the spring/summer season, recording SSTs from this period (e.g. Armand, 1997). This also implies that the distribution of GDGTs of Crenarchaeota might reflect more spring/summer rather than annual mean SSTs in (sub)polar ocean systems. In polar coastal waters, the abundance of Crenarchaeota is generally higher during the winter period (e.g. Murray et al., 1998; Church et al., 2003; Alonso-Sáez et al., 2008; Kalanetra et al., 2009). However, crenarchaeotal cells are too small (<1 μm, Margot et al., 2002), and thus not sufficiently dense, to sink as individual cells (Wakeham et al., 2003). Therefore, there must be a mechanism that results in transportation of crenarchaeotal cells to sediments such as fecal pellet or marine snow formation (cf. Huguet et al., 2006a). In the Arabian Sea, it has been suggested that the high flux of GDGTs during the productive summer monsoon is related to a more efficient food web-based scavenging of archaeal cells and not necessarily to higher crenarchaeotal cell abundances (Wuchter et al., 2006a). Similarly, in (sub)-polar oceans, crenarchaeotal cells may be more efficiently transported to sediments when the primary productivity is higher during the summer period and thus the formation of particle aggregates is higher in surface waters. Accordingly, GDGT-based indices may represent more spring/summer SST rather than annual mean SST. Alternatively, crenarchaeotal production at the core site might have been higher in summer than in winter during the last glacial period. Clearly, more work is needed to better understand the effect of seasonal skewing on GDGT index-1. In summary, it appears that for (sub)polar ocean systems, GDGT index-1 is more suitable for SST estimates than TEX_{86}, $1/TEX_{86}$, and GDGT index-2.

3.5.2. (Sub)tropical oceans

A GDGT dataset from Quaternary sediments from the Arabian Sea (10°47′N, 51°56′E, 1567 m water depth) spanning from the last glacial maximum (LGM) to the Late Holocene (Huguet et al., 2006b) was investigated as a test case for (sub)tropical oceans applying our new indices and calibration models. The previous SST reconstruction based on TEX_{86} using the Schouten et al. (2002) core top calibration resulted in a SST maximum of ~32 °C during the early Holocene and a warming of ~3 °C from the LGM to the Late Holocene (Huguet et al., 2006b). Overall, the new linear TEX_{86} calibration model (Eq. (5)) yields highest SST estimates among the new calibration models, especially with unrealistically high SST values (>30 °C) during the early Holocene (Fig. 8B). This indicates that the new linear TEX_{86} calibration model, which comprises the entire range of calibration temperature (−3 to 30 °C), is not appropriate for reconstructing SST for (sub)tropical oceans. The SST records reconstructed using the other three calibration models (Eqs. (6), (8), and (10)) show similar trends and SST estimates with core-top SST values close to the present-day annual mean SST in this area (~26 °C, Casey and Cornillon, 1999). Their maximum SSTs are lower (~30 °C or less) than those previously reconstructed by Huguet et al. (2006b). All three calibration models result in the same SST differences between the LGM and the modern SST (~2 °C). These estimates are similar to those reconstructed by the MARGO project members (2009) for the Indian Ocean based on a range of proxies. Although all new calibration models would yield similar SST variations, GDGT-index 2 is likely the most appropriate index for reconstructing SST for (sub)tropical oceans as the error of SST estimates is smaller using GDGT index-2 compared to GDGT index-1 (see above).

3.5.3. Greenhouse world oceans with SSTs beyond the calibration range

We also applied the new indices and calibration models to a GDGT dataset from sediments from the Paleocene–Eocene boundary from Wilson Lake in New Jersey (39°39′N, 75°03′W). This time interval is well known for extreme warmth and rapid changes in SST because of the massive input of isotopically light carbon such as methane to the atmosphere (e.g. Dickens et al., 1995). Zachos et al. (2006) applied TEX_{86} and found SSTs ranging from 27 to 33 °C at the Paleocene–Eocene boundary based on a "high temperature" calibration by Schouten et al. (2003). When we use an extrapolation of our new TEX_{86} calibration (Eq. (5)), SSTs vary between 27 and 49 °C, with a warming pulse of ~12 °C across the Paleocene–Eocene boundary (Fig. 8C). Especially, the peak SST of 49 °C is exceedingly high compared to the present-day annual mean SST (~14 °C, Casey and Cornillon, 1999) for this location and does not match SST estimates derived from the $\delta^{18}O$ of well-preserved planktonic foraminifera (~33 °C, Zachos et al., 2006). The SST record based on GDGT index-1 (Eq. (8)) ranges from 20 to 31 °C, which magnitude of SST change (8 °C) is similar to that estimated from $\delta^{18}O$ of planktonic foraminifera. However, background SST estimates (~21 °C) are probably too low, as they are only 4 °C

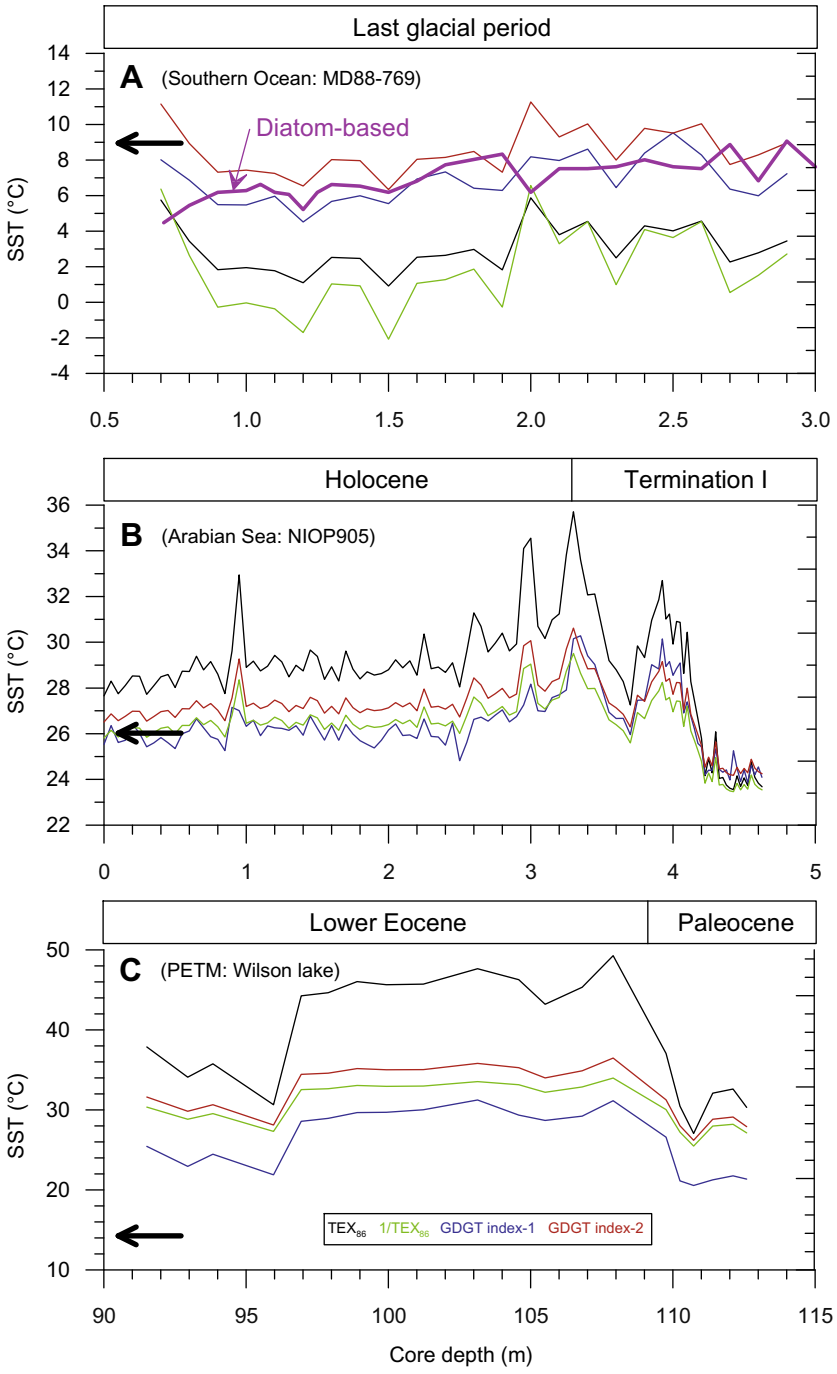

Fig. 8. Application of GDGT-based indices and calibrations to GDGT datasets from sediment cores covering different temperature ranges: (A) MD88-769 from the Southern Ocean (Kim et al., 2009), (B) NIOP905 from the Arabian Sea (Huguet et al., 2006b), and (C) Wilson lake core from the Paleocene–Eocene boundary (Zachos et al., 2006). Arrows indicate modern annual mean SSTs. The purple line indicates the diatom-based SST record from MD88-769.

higher than present day SST, whilst CO_2 levels during the Paleocene–Eocene Thermal Maximum may have been as high as 3000 ppmv (Pearson and Palmer, 2000). The application of Eq. (6)) derived from the reciprocal approach by Liu et al. (2009) as well as the GDGT-index-2 calibration yield roughly similar absolute SST estimates both before (ca. 26–27 °C) and after (33–34 °C) the Paleocene–Eocene boundary. These estimates are quite similar to those based on the $\delta^{18}O$ of planktonic foraminifera (Zachos et al., 2006). However, the maximum hypothetical temperature using the TEX_{86} reciprocal calibration is ~35 °C, whereas that with the GDGT index-2 calibration can yield values as high as ~39 °C. Furthermore, because the culture data better fit with the GDGT index-2 calibration line rather

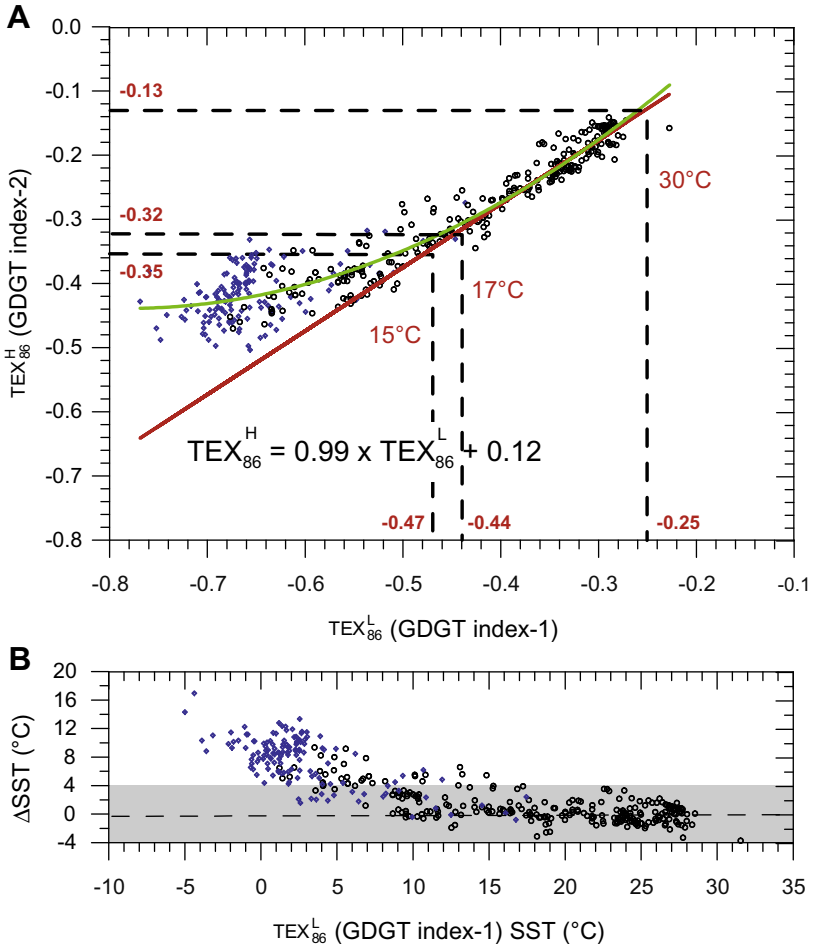

Fig. 9. A) Scatter plot of TEX_{86}^{L} (GDGT index-2) versus TEX_{86}^{H} (GDGT index-3). The red line is the linear regression line $TEX_{86}^{H} = 0.99 \times TEX_{86}^{L} + 0.12$, assuming that both TEX_{86}^{L} and TEX_{86}^{H} will result in the same temperature estimate. The green line is the second order polynomial regression line between TEX_{86}^{L} and TEX_{86}^{H} ($r^2 = 0.92$). B) ΔSST is the difference of the modeled SST derived from TEX_{86}^{L} (Eq. (8)) and TEX_{86}^{H} (Eq. (10)) calibration models, respectively. The grey shaded area indicates the residual standard error of the GDGT index-1 calibration model, Eq. (8) (±4 °C). Symbols and colors are as in Fig. 2B. (For interpretation of the references to colour in this figure legend, the reader is referred to the web version of this article.)

than the reciprocal calibration line of TEX_{86} (see the discussion above), it seems that GDGT index-2 may be more suitable than the other calibration models for reconstructing SST in tropical oceans where SSTs were much higher than today, outside the range of our calibration dataset (>30 °C).

4. IMPLICATIONS

The findings of our study have several implications for the application of GDGT distribution to reconstruct past SST. For the (sub)polar oceans, the regio-isomer of crenarchaeol does not seem to be of considerable importance in the membrane adaptation of Marine Group I Crenarchaeota to temperature. Therefore, it appears that the use of GDGT index-1, which does not contain the crenarchaeol regio-isomer, is more appropriate for SST estimates of low-temperature oceans. We propose to name this GDGT index-1 TEX_{86}^{L}, where L stands for low temperature regions. In contrast, for the (sub)tropical oceans and greenhouse periods where SST was substantially higher than today (>30 °C), the crenarchaeol regio-isomer seems to play a much more important role for temperature adaptation. The extrapolation of the GDGT index-2 calibration line provides expected amplitude changes in temperature as well as realistic absolute temperature estimates compared to other proxies (Fig. 8). As a result, the application of GDGT index-2 is most appropriate for GDGT-based paleothermometry of (sub)tropical and greenhouse world oceans. This index is similar to the original TEX_{86} definition (Schouten et al., 2002), except that it is now based on a logarithmic function. We propose to name GDGT index-2 TEX_{86}^{H}, where H stands for high temperature regions.

For most paleo-SST reconstructions, it will be clear which index and corresponding calibration model should be used. However, in certain cases such as (sub)polar oceans in a greenhouse world, or (sub)tropical oceans in an icehouse world, it may be less certain which calibration model should be used. To address this issue, we compared how well TEX_{86}^{L} and TEX_{86}^{H} predict temperature in the

present day oceans. We first plotted TEX_{86}^{L} and TEX_{86}^{H} values of all the core-top sediments (Fig. 9A). If TEX_{86}^{L} and TEX_{86}^{H} would predict the exact same SST, Eqs. (8) and (10)) can be combined. The resulting equilibrium line is then as follows:

$$TEX_{86}^{H} = 0.99 \times TEX_{86}^{L} + 0.12 \quad (11)$$

This line is plotted in Fig. 9A and represents the line, where TEX_{86}^{L} and TEX_{86}^{H} values predict the same SST. For the temperature range between 17 and 30 °C, corresponding to the index values of −0.44 and −0.25 for TEX_{86}^{L} and of −0.32 and −0.13 for TEX_{86}^{H}, respectively, both indices predict SST quite well. However, below 17 °C most points of core top sediments are plotted above the line. This is primarily due to the overestimation of SST with TEX_{86}^{H}. These observations can also be visualized by computing the difference of the modeled SST (ΔSST), i.e. TEX_{86}^{H} SST minus TEX_{86}^{L} SST (Fig. 9B). The modeled SSTs using both indices are well within the residual standard error of the TEX_{86}^{L} calibration model (±4 °C) between 15 and 30 °C. Below 15 °C, the TEX_{86}^{H} calibration model starts to overestimate SST beyond the residual standard error of TEX_{86}^{L} calibration model. This suggests that the TEX_{86}^{H} calibration model is suitable to reconstruct SSTs above 15 °C but not below 15 °C. For cases where paleorecords encompass temperatures both below and above 15 °C, it is suggested to use TEX_{86}^{L} as this gives similar SST estimates as TEX_{86}^{H} though with a slightly larger error.

ACKNOWLEDGEMENTS

We would like to thank J. Ossebaar for assistance with the HPLC/APCI-MS. D. Klitgaard Kristensen, the participants and the crew of the SciencePub IPY-cruise in 2007 on the R/V Lance from the Norwegian Polar Institute are appreciated for their help for the Svalbard surface sediment sampling. We are grateful to various people who provided core-top sediments for this study: E. Domack (Hamilton College), S. Jacobs (LDEO), A. Leventer (Colgate University), A. deVernal (UQAM), J. Knies (NGU), and C. Slomp and S. N. Fhlaithearta (Utrecht University). We thank associate editor J. Werne, and A. Ingalls, and an anonymous reviewer for constructive comments.

APPENDIX A. SUPPLEMENTARY DATA

Supplementary data associated with this article can be found, in the online version, at doi:10.1016/j.gca.2010.05.027.

REFERENCES

Armand L. (1997) The use of diatom transfer functions in estimating sea-surface temperature and sea-ice in cores from the southeast Indian Ocean. Ph. D Thesis, Australian National University, Canberra, Australia, p. 932.

Alonso-Sáez L., Sánchez O., Gasol J. M., Balagué V. and Pedrós-Alio C. (2008) Winter-to-summer changes in the composition and single-cell activity of near-surface Arctic prokaryotes. *Environ. Microbiol.* **10**, 2444–2454.

Blumenberg M., Seifert R., Reitner J., Pape T. and Michaelis W. (2004) Membrane lipid patterns typify distinct anaerobic methanotrophic consortia. *Proc. Natl. Acad. Sci. USA* **101**, 11111–11116.

Brown P. J. (1993) *Measurement, Regression And Calibration*. Clarendon Press, Oxford.

Casey K. and Cornillon P. (1999) A comparison of satellite and in situ-based sea surface temperature climatologies. *J. Climate* **12**, 1848–1863.

Church M. J., DeLong E. F., Ducklow H. W., Karner M. B., Preston C. M. and Karl D. M. (2003) Abundance and distribution of planktonic Archaea and Bacteria in the waters west of the Antarctic Peninsula. *Limnol. Oceanogr.* **48**, 1893–1902.

Dickens G. R., O'Neil J. R., Rea D. K. and Owen R. M. (1995) Dissociation of oceanic methane hydrate as a cause of the carbon isotope excursion at the end of the Paleocene. *Paleoceanography* **10**, 965–971.

Hatzenpichler R., Lebecleva E. V., Spieck E., Stoecker K., Richter A., Daims H. and Wagner M. (2008) A moderately thermophilic ammonia-oxidizing crenarchaeote from a hot spring. *Proc. Natl. Acad. Sci. USA* **105**, 2134–2139.

Herfort L., Schouten S., Boon J. P. and Sinninghe Damsté J. S. (2006) Application of the TEX_{86} temperature proxy in the southern North Sea. *Org. Geochem.* **37**, 1715–1726.

Herndl G. J., Reinthaler T., Teira E., van Aken H., Veth C., Pernthaler A. and Pernthaler J. (2005) Contribution of Archaea to total prokaryotic production in the deep Atlantic Ocean. *Appl. Environ. Microbiol.* **71**, 2303–2309.

Hopmans E. C., Schouten S., Pancost R. D., Van Der Meer M. J. T. and Sinninghe Damsté J. S. (2000) Analysis of intact tetraether lipids in archaeal cell material and sediments using high performance liquid chromatography/atmospheric pressure ionization mass spectrometry. *Rap. Comm. Mass. Spectrum* **14**, 585–589.

Hopmans E. C., Weijers J. W. H., Schefuß E., Herfort L., Sinninghe Damsté J. S. and Schouten S. (2004) A novel proxy for terrestrial organic matter in sediments based on branched and isoprenoid tetraether lipids. *Earth Plan. Sci. Lett.* **224**, 107–116.

Huguet C., Cartes J. E., Sinninghe Damsté J. S. and Schouten S. (2006a) Marine crenarchaeotal membrane lipids in decapods: Implications for the TEX_{86} paleothermometer. *Geochem. Geophys. Geosyst.*. doi:10.1029/2006GC001305.

Huguet C., Kim J.-H., Sinninghe Damsté J. S. and Schouten S. (2006b) Reconstruction of glacial-interglacial sea surface temperature in the Arabian Sea using organic proxies. *Paleoceanography* **21**, PA300S. doi:10.1029/2005PA001215.

Huguet C., Schimmelmann A., Thunell R., Lourens L. J., Sinninghe Damsté J. S. and Schouten S. (2007a) A study of the TEX_{86} paleothermometer in the water column and sediments of the Santa Barbara Basin California. *Paleoceanography*. doi:10.1029/2006PA001310.

Huguet C., Schimmelmann A., Thunell R., Lourens L. J., Sinninghe Damsté J. S. and Schouten S. (2007b) A study of the TEX_{86} paleothermometer in the water column and sediments of the Santa Barbara Basin, California. *Paleoceanography*. doi:10.1029/2006PA001310.

Kalanetra K. M., Bano N. and Hollibaugh J. T. (2009) Ammonia-oxidizing Archaea in the Arctic Ocean and Antarctic coastal waters. *Environ. Microbiol.*. doi:10.1111/j.1462-2920.2009.01974.x.

Karner M., DeLong E. F. and Karl D. M. (2001) Archaeal dominance in the mesopelagic zone of the Pacific Ocean. *Nature* **409**, 507–510.

Kim J.-H., Schouten S., Hopmans E. C., Donner B. and Sinninghe Damsté J. S. (2008) Global sediment core-top calibration of the TEX_{86} paleothermometer in the ocean. *Geochim. Cosmochim. Acta* **72**, 1154–1173.

Kim J.-H., Crosta X., Michel E., Schouten S., Duprat J. and Sinninghe Damsté J. S. (2009) Impact of lateral transport on organic proxies in the Southern Ocean. *Quat. Res.* **71**, 246–250.

Koga Y., Nishihara M., Morii H. and Akagawa-Matsushita M. (1993) Ether polar lipids of methanogenic bacteria: structures, comparative aspects, and biosyntheses. *Microbiol. Rev.* **57**, 164–182.

Lee K.-E., Kim J.-H., Wilke I., Helmke P. and Schouten S. (2008) U37, TEX86, and planktonic foraminifera in the Benguela upwelling system: implications for past sea surface temperature estimates. *Geochem. Geophys. Geosyst.* **9**, Q10019. doi:10.1029/2008GC002056.

Lipp J. S., Morono Y., Inagaki F. and Hinrichs K.-U. (2008) Significant contribution of Archaea to extant biomass in marine subsurface sediments. *Nature* **454**, 991–994.

Lipp J. S. and Hinrichs K.-U. (2009) Structural diversity and fate of intact polar lipids in marine sediments. *Geochim. Cosmochim. Acta*. doi:10.1016/j.gca.2009.08.003.

Liu Z., Pagani M., Zinniker D., DeConto R., Huber M., Brinkhuis H., Shah S. R., Leckie R. M. and Pearson A. (2009) Global cooling during the Eocene–Oligocene climate transition. *Science* **323**, 1187–1190.

Project Members M. A. R. G. O. (2009) Constraints on the magnitude and patterns of ocean cooling at the Last Glacial Maximum. *Nature Geoscience* **2**, 127–132.

Margot H., Acebal C., Toril E., Amils R. and Fernández J. L. (2002) Consistent association of crenarchaeal *Archaea* with sponges of genus. *Axinella. Mar. Biol.* **140**, 739–745.

Mollenhauer G., Inthorn M., Vogt T., Zabel M., Sinninghe Damsté J. S. and Eglinton T. I. (2007) Aging of marine organic matter during cross-shelf lateral transport in the Benguela upwelling system revealed by compound-specific radiocarbon dating. *Geochem. Geophys. Geosyst.*. doi:10.1029/2007GC001603.

Mollenhauer G., Eglinton T. I., Hopmans E. C. and Sinninghe Damsté J. S. (2008) A radiocarbon-based assessment of the preservation characteristics of crenarchaeol and alkenones from continental margin sediments. *Org. Geochem.* **39**, 1039–1045.

Montgomery D. C. and E. A. Peck (1992) Introduction to Linear Regression Analysis. 2nd ed. John Wiley & Sons, New York.0020.

Murray A. E., Preston C. M., Massana R., Taylor L. T., Blakis A., Wu K. and DeLong E. F. (1998) Seasonal and spatial variability of bacterial and archaeal assemblages in the coastal waters near Anvers Island, Antarctica. *Appl. Environ. Microbiol.* **64**, 2585–2595.

Pancost R. D., Hopmans E. C., Sinninghe Damsté J. S. and the MEDINAUT Shipboard Scientific Party (2001) Archaeal lipids in Mediterranean cold seeps: molecular proxies for anaerobic methane oxidation. *Geochim. Cosmochim. Acta* **65**, 1611–1627.

Pearson P. N. and Palmer M. R. (2000) Atmospheric carbon dioxide concentrations over the past 60 million years. *Nature* **406**, 695–699.

Pitcher A. S., Rychlik N., Hopmans E. C., Spieck E., Rijpstra W. I. C., Ossebaar J., Schouten S., Wagner M. and Sinninghe Damsté J. S. (2010) Crenarchaeol and its regioisomer dominate the membrane lipids of 2 "*Candidatus* Nitrososphaera gargensis" a thermophilic Group I.1b Crenarchaeote. *ISME J.* **4**, 542–552.

R Development Core Team (2008) R A language and environment for statistical computing. R Foundation for Statistical Computing, Vienna, Austria. ISBN 3-900051-07-0, URL http://www.R-project.org.

Schouten S., Hopmans E. C., Pancost R. D. and Sinninghe Damsté J. S. (2000) Widespread occurrence of structurally diverse tetraether membrane lipids: evidence for the ubiquitous presence of low-temperature relatives of hyperthermophiles. *Proc. Natl. Acad. Sci. USA* **97**, 14421–14426.

Schouten S., Hopmans E. C., Schefuß E. and Sinninghe Damsté J. S. (2002) Distributional variations in marine crenarchaeotal membrane lipids: A new organic proxy for reconstructing ancient sea water temperatures? *Earth Planet. Sci. Lett.* **204**, 265–274.

Schouten S., Hopmans E. C., Kuypers M. M. M., Van Breugel Y., Forster A. and Sinninghe Damsté J. S. (2003) Extremely high sea water temperatures at low latitudes during the middle Cretaceous as revealed by archaeal membrane lipids. *Geology* **31**, 1069–1072.

Schouten S., Forster A., Panato E. and Sinninghe Damsté J. S. (2007a) Towards the calibration of the TEX_{86} paleothermometer in ancient green house worlds. *Org. Geochem.* **38**, 1537–1546.

Schouten S., Huguet C., Hopmans E. C., Kienhuis M. and Sinninghe Damsté J. S. (2007b) Analytical Methodology for TEX_{86} paleothermometry by high-performance liquid chromatography/atmospheric pressure chemical ionization-mass spectrometry. *Anal. Chem.* **79**, 2940–2944.

Schouten S., Hopmans E. C., Baas M., Boumann H., Standfest S., Könneke M., Stahl D. A. and Sinninghe Damsté J. S. (2008) Intact membrane lipids of Candidatus "*Nitrosopumilus maritimus*", a cultivated representative of the cosmopolitan mesophilic Group I Crenarchaeota. *Appl. Env. Microbiol.* **74**, 2433–2440.

Sinninghe Damsté J. S., Hopmans E. C., Schouten S., Van Duin A. C. T. and Geenevasen J. A. J. (2002) Crenarchaeol: the characteristic core glycerol dibiphytanyl glycerol tetraether membrane lipid of cosmopolitan pelagic crenarchaeota. *J. Lipid Res.* **43**, 1641–1651.

Shah S. R., Mollenhauer G., Ohkouchi N., Eglinton T. I. and Pearson A. (2008) Origins of archaeal tetraether lipids in sediments: Insights from radiocarbon analysis. *Geochim. Cosmochim. Acta* **72**, 4577–4594.

Trommer G., Siccha M., van der Meer M. T. J., Schouten S., Sinninghe Damsté J. S., Schulz H., Hemleben C. and Kucera M. (2009) Distribution of Crenarchaeota tetraether membrane lipids in surface sediments from the Red Sea. *Org. Geochem.* **40**, 724–731.

Wakeham S. G., Lewis C. M., Hopmans E. C., Schouten S. and Sinninghe Damsté J. S. (2003) Archaea mediate anaerobic oxidation of methane in deep euxinic waters of the Black Sea. *Geochim. Cosmochim. Acta* **67**, 1359–1374.

Weijers J. W. H., Schouten S., Spaargaren O. C. and Sinninghe Damsté J. S. (2006) Occurrence and distribution of tetraether membrane in soils: Implications for the use of the BIT index and the TEX_{86} SST proxy. *Org. Geochem.* **37**, 1680–1693.

Weijers J. W. H., Schouten S., van den Donker J. C., Hopmans E. C. and Sinninghe Damsté J. S. (2007) Environmental controls on bacterial tetraether membrane lipid distribution in soils. *Geochim. Cosmochim. Acta* **71**, 703–713.

Wuchter C., Schouten S., Coolen M. J. L. and Sinninghe Damsté J. S. (2004) Temperature-dependent variation in the distribution of tetraether membrane lipids of marine Crenarchaeota: implications for TEX_{86} paleothermometry. *Paleoceanography* **19**, PA4028. doi:10.1029/2004PA001041.

Wuchter C., Schouten S., Wakeham S. G. and Sinninghe Damsté J. S. (2005) Temporal and spatial variation in tetraether membrane lipids of marine Crenarchaeota in particulate organic matter: implication for TEX_{86} paleothermometry. *Paleoceanography* **20**, PA3013. doi:10.1029/2004PA001110.

Wuchter C., Abbas B., Coolen M. J. L., Herfort L., Timmers P., Strous M., van Bleijswijk J., Teira E., Herndl G. J., Middelburg J. J., Schouten S. and Sinninghe Damsté J. S. (2006a) Archaeal

nitrification in the ocean. *Proc. Nat. Acad. Sci. USA* **103**, 12317–12322.

Wuchter C., Schouten S., Wakeham S. G. and Sinninghe Damsté J. S. (2006b) Archaeal tetraether membrane lipid fluxes in the northeastern Pacific and the Arabian Sea: implications for TEX_{86} paleothermometry. *Paleoceanography* **21**, PA4208. doi:10.1029/2006PA001279.

Zachos J. C., Schouten S., Bohaty S., Quattlebaum T., Sluijs A., Brinkhuis H. and Sloan L. C. (2006) Extreme warming of mid-latitude coastal ocean during the Paleocene–Eocene thermal maximum: inferences from TEX_{86} and isotope data. *Geology* **34**, 737–740.

Associate editor: Josef Werne